Small-angle neutron scattering of phase separation in amorphous $Zr_{41}Ti_{14}Cu_{12.5}Ni_{10}Be_{22.5}$ alloy

1997 J. Phys.: Condens. Matter 9 2731

(http://iopscience.iop.org/0953-8984/9/13/010)

J. Phys.: Condens. Matter **9** (1997) 2731–2738. Printed in the UK PII: S0953-8984(97)77315-6

Small-angle neutron scattering of phase separation in amorphous $Zr_{41}Ti_{14}Cu_{12.5}Ni_{10}Be_{22.5}$ alloy

Jun-Ming Liu†‡§, A Wiedenmann†, U Gerold†, U Keiderling† and H Wollenberger†

† Hahn-Meitner-Institut Berlin, Bereich NM, Glienicker Straße 100, 14109 Berlin, Germany
‡ Laboratory of Solid State Microstructures, Nanjing University, Nanjing 210093, People's Republic of China

Received 21 August 1996

Abstract. Phase separation in the amorphous $Zr_{41}Ti_{14}Cu_{12.5}Ni_{10}Be_{22.5}$ alloy annealed at 620 and 643 K has been investigated by means of the *in situ* small-angle neutron scattering (SANS) technique. The alloy decomposes into two supercooled liquid phases, with the volume fraction of about 10–20% for the second phase. The interphase boundary causes q^{-4} scattering behaviour. The phase separation rate depends strongly on temperature, with a rather sluggish coarsening in the late stage. The kinetic exponent of this coarsening stage was found to be about 0.06, to be compared with the Lifshitz–Wagner exponent, 0.33.

Bulk metallic glasses prepared by means of rapid solidification are of special interest, not only from the point of view of advanced engineering applications, but also as representative objects for fundamental studies of relaxation processes in matter far from equilibrium. Recently, a series of large-size bulk metallic glasses with a complex multicomponent chemistry was developed [1, 2]. They exhibit many excellent mechanical and physical properties, of which the high thermal stability against crystallization and complicated behaviours of phase transitions in the supercooled liquid range have been paid special attention in recent research activities [3–6].

Amorphous $Zr_{41}Ti_{14}Cu_{12.5}Ni_{10}Be_{22.5}$ represents one of the alloys which have been intensively studied in the last 2 years [6–10]. Amorphous samples of 10 mm diameter can be obtained by means of the current solidification method as long as a quenching rate of $\sim$10 K s^{-1} is achieved. It was found that above its glass transition temperature ($T_g \approx 620$ K) this alloy exhibits a wide supercooled liquid range (roughly from 620 to 673 K), in which a complicated diffusion behaviour associated with a phase separation was discovered [9–11]. It was demonstrated that the phase separation considerably improved the thermal stability of this alloy against subsequent crystallization [10]. Depending on the thermal history the alloy acquired different microstructures consisting of nano-sized crystalline phases embedded in supercooled liquid matrix, or two supercooled liquid phases with one phase being nano-sized particles and differing from the matrix in their Be and Ti contents [9]. The microstructure achieved by heating up to temperatures above the crystallization temperature, after a full relaxation in the supercooled liquid range, is significantly different from that slowly solidified from the melt or that resulting from rapid heating from the amorphous state [9].

§ Corresponding author.

0953-8984/97/132731+08$19.50

Some experimental investigations on the phase separation by means of transmission electron microscopy (TEM) [9, 12], small-angle neutron scattering (SANS) [10, 12] and atom-probe field ion microscopy (APFIM) [7, 9] were carried out. As observed by TEM, the amorphous sample annealed in the supercooled liquid range showed two diffraction rings which were separated from each other and also the dark-field image exhibited visible contrast reflecting the nano-sized amorphous clusters of one phase embedded in the matrix [9]. The SANS measurements revealed a distinct peak of the scattering curve and peak shifting toward the small-wave-vector range with increasing annealing time. Contrary to the finding by Schneider *et al* [12] that the phase separation initiated after a long incubation period and produced nano-crystals embedded in the amorphous matrix, Wiedenmann *et al* [10] observed the phase separation immediately after the amorphous sample was heated up to the supercooled liquid range and no contribution from nano-sized crystals to the scattering was detected. The atom probe revealed composition fluctuations during the phase separation and showed anti-correlated fluctuations of Ti and Be [9]. The anomalous diffusion of Be was suggested to be the limiting step of the process [8].

In the present paper, we investigate the time evolution of the phase separation in the alloy annealed at $T = 620$ and 643 K, by using the *in situ* SANS technique, focusing on the kinetics.

The bulk samples of amorphous $Zr_{41}Ti_{14}Cu_{12.5}Ni_{10}Be_{22.5}$ alloy were prepared by remelting the solidified ingots with nominal constitution in sealed silica tubes containing pure Ar at a pressure greater than 1.0 atm and subsequent quenching into water. The amorphous state of the samples was confirmed by x-ray diffraction and TEM. The supercooled liquid state of this alloy, ranging from 620 to 673 K, was determined by using differential scanning calorimetry (DSC) [9], although this range may vary a little depending on the heating rate for DSC measurement. The *in situ* SANS experiment was performed in the V4 instrument installed in the BER-II reactor at the Hahn-Meitner-Institut Berlin, Germany [13]. Neutrons with a wavelength, λ, of 0.6 nm and a resolution $\Delta\lambda/\lambda = 10.8$ were used and the sample–detector distance varied between 1.21 and 8.00 m, with the momentum transfer (wave-vector in the scattering geometry), q, covering the range of $0.03\ \mathrm{nm}^{-1} < q < 2.00\ \mathrm{nm}^{-1}$, because the spatial variations in scattering length density in the sample ranged from a few nanometres to more than ten nanometres. The disc-like samples 10 mm in diameter and 1.0 mm in thickness were individually placed into a furnace installed in the SANS spectrometer.

During the measurements, each sample was annealed at the nominal temperature after heating up from room temperature within 2 min. The two-dimensional neutron detector was cycled between the two given distances with a data acquisition time of about 5 min at each position and with a moving time of 3 min between the two positions. Before heating and after prolonged annealing of the sample, the detector was positioned up to 8.00 m and even up to 16.00 m from the sample in order to collect scattering data in the small-q range (down to $0.03\ \mathrm{nm}^{-1}$). After corrections for the background, transmission and efficiency of the detector, the scattering intensity $S(q, t)$ was obtained as a function of the time of anneal t. The scattering profile was found to be perfectly isotropic. Therefore, the data presented below were an azimuthal average of the scattering contours derived by referring to the scaling of the intensity of a standard sample of water. $S(q, t)$ was derived in units of cm^{-1}.

Figures 1 and 2 present the time evolution of the scattering intensity function, $S(q, t)$, for samples annealed at $T = 620$ and 643 K, respectively. The extrapolations to $S(0, t) = 0$ in figure 2 were confirmed by very low-q-range measurements of the scattering. For each long-time annealed sample, $S(q, t) < 2\times10^{-3}\ \mathrm{cm}^{-1}$ was found for $q < 0.04\ \mathrm{nm}^{-1}$. Because crystallization of this alloy causes a strong increase of $S(q, t)$ at small values of q (e.g.

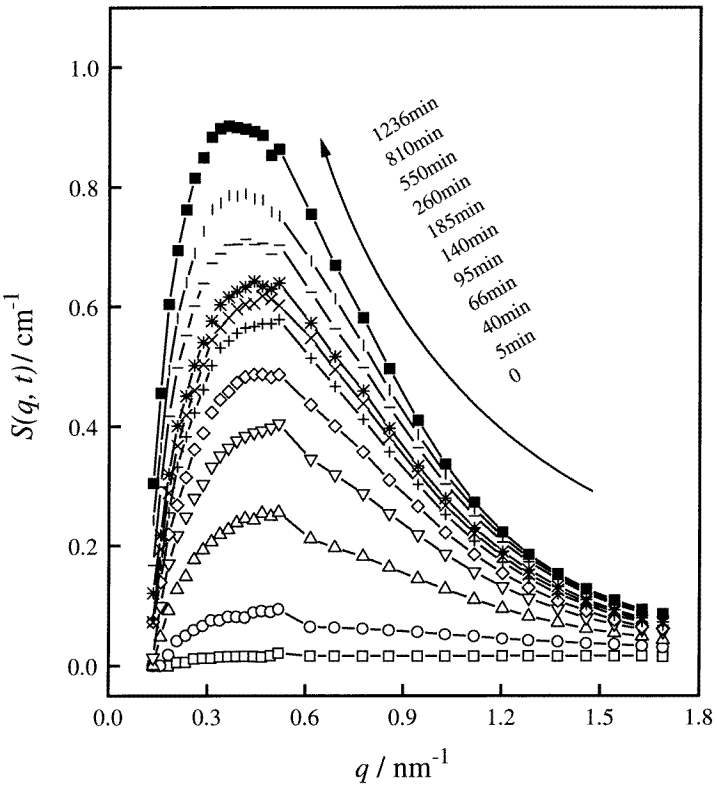

Figure 1. Neutron scattering curves of amorphous $Zr_{41}Ti_{14}Cu_{12.5}Ni_{10}Be_{22.5}$ annealed at $T = 620$ K for the time periods indicated.

$q < 0.3$ nm^{-1}) to values $S(q,t) > 10$ cm^{-1}, this behaviour excludes any crystallization during this heat treatment, The scattering intensity depends strongly on temperature. For equal annealing period, the scattering peak intensity at $T = 643$ K is almost ten times that for $T = 620$ K.

The scattering patterns indicate the presence of a specific phase separation since there is a rapid increase in intensity and a shift in the peak intensity just after reaching the annealing temperature. Later, the rate of change of $S(q,t)$ decreases steeply.

At large q values, $S(q)$ can well be fitted to Porod's q^{-4} law [14] for all samples annealed at the two temperatures. For a further characterization of the phase separation, we derive specific structural parameters from the scattering curves. We define the nth moment $S_n(t)$ and its normalized form $q_n(t)$ of the scattering as

$$\begin{aligned} S_n(t) &= \int_0^{q_L} q^n S(q,t)\,\mathrm{d}q + \int_{q_L}^{\infty} a q^{n-4}\,\mathrm{d}q \qquad n = 0, 1, 2 \\ q_n(t) &= S_n(t)/S_0(t) \qquad n = 1, 2 \end{aligned} \tag{1}$$

where q_L is the cutoff for large q and a is a positive constant which was obtained by fitting the data near q_L with the q^{-4} law in order to compensate for the error arising from the large-q cutoff. Obviously, q_1 scales the characteristic length of the phase separating microstructure. $S_2(t)$ actually is the invariant of the scattering, which can be written as

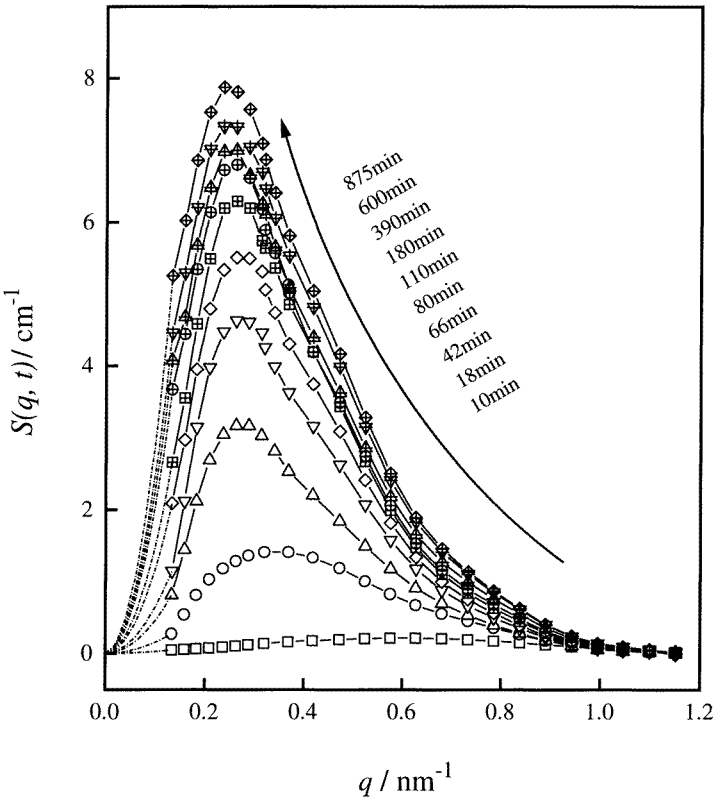

Figure 2. Neutron scattering curves of amorphous $Zr_{41}Ti_{14}Cu_{12.5}Ni_{10}Be_{22.5}$ annealed at $T = 643$ K for the time periods indicated. The dashed lines for $q < 0.1$ nm^{-1} are eye-fit extrapolations to $S = 0$.

[13]:

$$S_2 = 2\pi^2 \Delta\eta^2 \phi(1-\phi) \tag{2}$$

with the contrast factor

$$\Delta\eta = \left(\sum_i c_i b_i \rho_M\right)_M - \left(\sum_i c_i b_i \rho_P\right)_P \tag{3}$$

where c_i is the atomic concentration and b_i the scattering length of species i, $\rho_{i=M \text{ and } P}$ the atomic density of matrix and precipitate; the subscripts M and P denote matrix and precipitate, and ϕ is the volume fraction of the precipitates. Evaluation of the contrast factor as a function of time is crucial because this factor scales the amplitude of the compositional fluctuation associated with the phase separation.

Furthermore, the Guinier approximation holds in a wide q range above the maximum, which allows R_g, the radius of gyration for the precipitates, to be obtained according to

$$S(q,t) = S_0 \exp(-R_g^2 q^2/3) \tag{4}$$

with S_0 being a positive constant.

The evaluated parameters, q_1, R_g and S_2 are presented in figure 3. Obviously, the time evolution of the decomposition is characterized by two regimes with a transition period

between 50 and 150 min independent of temperature between 620 and 643 K. In the initial regime, all three parameters change rapidly, while in the final regime the process seems to proceed very sluggishly.

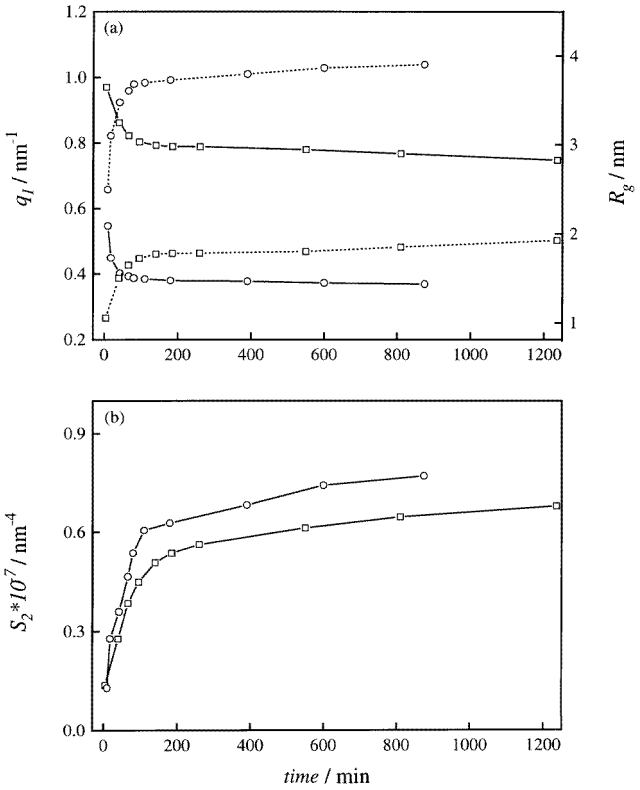

Figure 3. (a) Characteristic wave-vector q_1 (solid lines) and radius of gyration R_g (dashed lines) and (b) second-order moment S_2 as functions of annealing time at $T = 620$ K (squares) and 643 K (circles) for amorphous $Zr_{41}Ti_{14}Cu_{12.5}Ni_{10}Be_{22.5}$.

The geometrical parameters q_1 and R_g depend strongly on temperature, while S_2 does not. The characteristic length $2\pi/q_1$ of the decomposition structure is larger by at least a factor of 4.5 than R_g, indicating isolated precipitates embedded in the matrix.

By assuming a narrow size distribution of precipitates, the characteristic length q_1 becomes the average inter-particle distance and hence the precipitate density is given by

$$N_p = (q_1/2\pi)^3. \tag{5a}$$

The volume of the precipitate, V_p, and the volume fraction of all droplets, ϕ, can then be written as

$$V_p = 4\pi\theta R_g^3/3 \tag{5b}$$

$$\phi = N_p V_p \tag{5c}$$

where $\theta = (5/3)^{3/2}$ for spherical precipitates. Then the squared contrast factor $\Delta\eta^2$ can be evaluated from S_2 according to (2). The resulting quantities V_p, ϕ, N_p and $\Delta\eta^2$ are plotted in figure 4(a)–4(d), respectively, against annealing time. The precipitate volume and

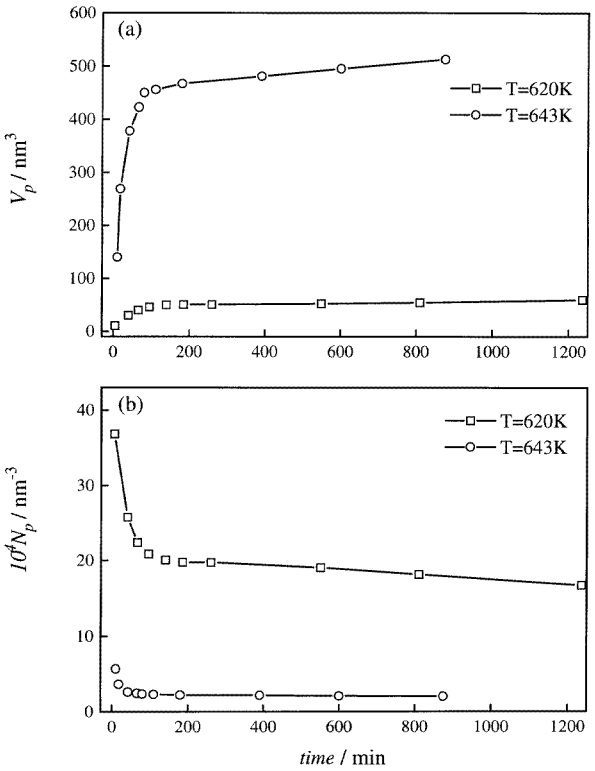

Figure 4. The annealing time dependence of (a) the average volume V_p, (b) the density N_p, (c) the volume fraction ϕ and (d) the contrast factor $\Delta\eta^2$ at $T = 620$ and 643 K, for amorphous $Zr_{41}Ti_{14}Cu_{12.5}Ni_{10}Be_{22.5}$.

the density depend strongly on temperature while the volume fraction does not. From the difference in scattering contrast $\Delta\eta^2$ at the two temperatures in figure 4(d) one concludes an enhanced deviation of the compositions of the two phases at the higher temperature. One must keep in mind, however, that $\Delta\eta^2$ is very sensitive to the elemental distribution and a redistribution of one constituent by just 3 at.% would explain the difference shown in figure 4(d).

The continuous increase of $\Delta\eta^2$ for $t < 200$ min resembles the characteristics of a spinodal decomposition. The same is true for the pattern of N_p (figure 4(b)). For a nucleation mode one would expect an initial increase of N_p with increasing annealing time. However, it is not quite clear whether the initial decrease of q_1 (figure 4(a)) which leads to the increase of ϕ and finally to the increase of $\pi\Delta\eta^2$ in figure 4(d) is really caused by an increase of the average distance of the precipitates or not. Recent computer simulations of a germ-grained model with a hard-core structure has shown that q_m decreases slightly with increasing volume fraction even when the mean particle distance remains constant. The implication for this behaviour on q_1 is not known, however [15]. Hence, we may conclude that if the initial decrease of q_1 (figure 4(a)) reflects the inter-particle distance correctly the behaviour of $\pi\Delta\eta^2$ will demonstrate the spinodal decomposition mode.

The value of ϕ can be estimated in the late stage following the approach proposed by

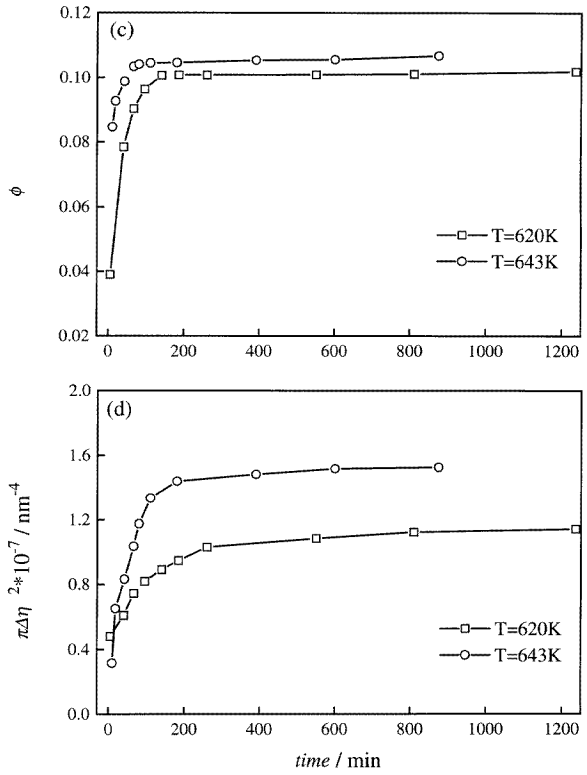

Figure 4. (Continued)

Fratzl and Lebowitz [16, 17]. The calculation shows that for the phase separation at both 620 and 643 K the late stage's volume fraction is about 0.06 ± 0.02. As the intensity function follows an exponent smaller than 4.0 for small values of q, the Fratzl–Lebowitz approach [16, 17] certainly underestimates the volume fraction. A direct calculation of ϕ from the atom-probed constitution of the two phases [9] according to (2) and (3) yields $\phi \approx 0.20$.

Finally, we go back to the kinetics of phase separation. In figure 5 the time behaviour of R_g is shown in a double-log plot. In the initial stage, the few data may be approximated by a power law with exponent $k \approx 0.20$–0.25, and in the late stage we have $k = 0.06$ at $T = 620$ K and 0.05 at $T = 643$ K. Diffusion measurements in this alloy [18] revealed that the diffusivity of elements Al (faster than Ti and Zr) and Co (similar to Ni) slows down during decomposition in the supercooled liquid state. Small values of k for phase separation have been obtained also in other systems, such as AlSi alloys ($k \approx 0.08$) [19] and AlZnMg alloys ($k \approx 0.08$) [20]. A preferable explanation for the anomalous behaviour in the two systems is the presence of a strong constitutional and mechanical dependence of the diffusion of some elements during phase separation.

In conclusion, the small-angle neutron scattering investigation of phase separation in amorphous $Zr_{41}Ti_{14}Cu_{12.5}Ni_{10}Be_{22.5}$ has been carried out. It has been observed that on reaching the supercooled liquid range the amorphous alloy decomposes into two supercooled liquids via a spinodal-like mode. The precipitates occupy a low volume fraction of about 10%. The microstructural evolution exhibits strong temperature dependence. The kinetic

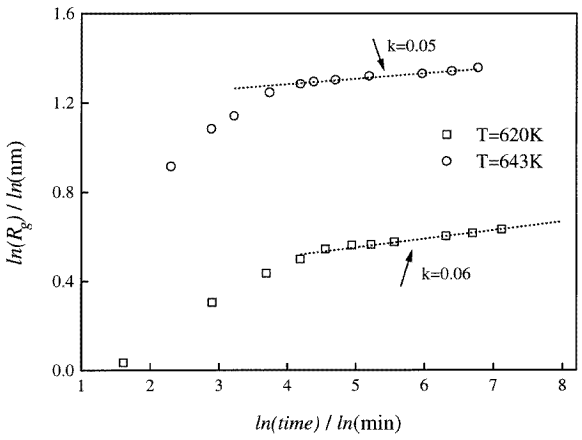

Figure 5. The radius of gyration R_g plotted against time in log–log scales, for phase separation of amorphous $Zr_{41}Ti_{14}Cu_{12.5}Ni_{10}Be_{22.5}$ at $T = 620$ and 643 K. The straight lines represent the power function fittings.

exponent for coarsening in the late stage was found to be about 0.06, probably due to strong constitutional dependence of diffusivity of the elements during phase separation.

Acknowledgments

One of the authors (J-ML) would like to thank the Alexander von Humboldt Foundation for financial support of the present work. The authors acknowledge the help and comments from Dr M-P Macht, Dr J Kohlbrecher, Dr E Budke and Ms Q Wei.

References

[1] Inoue A, Zhang T and Masumoto T 1990 *Mater. Trans. JIM* **31** 177
[2] Peker A and Johnson W L 1993 *Appl. Phys. Lett.* **63** 2342
[3] Inoue A, Zhang T and Masumoto T 1990 *Mater. Trans. JIM* **36** 391
[4] Johnson W L and Peker A 1995 *Science and Technology of Rapid Solidification and Processing* ed M A Otooni (Deventer: Kluwer) p 25
[5] Greer A L 1993 *Nature* **366** 6453
[6] Kim Y J, Busch R, Johnson W L, Rulison A J and Rhim W K 1994 *Appl. Phys. Lett.* **65** 2136
[7] Busch R, Kim Y J, Johnson W L, Rulison A J, Rhim W K and Isheim D 1995 *Appl. Phys. Lett.* **66** 3111
[8] Geyer U, Schneider S, Johnson W L, Qiu Y, Tombrello T A and Macht M P 1995 *Phys. Rev. Lett.* **75** 2364
[9] Macht M P, Wanderka N, Wiedenmann A, Wollenberger H, Wei Q, Fecht H J and Klose S G 1996 *Mater. Sci. Forum* at press
[10] Wiedenmann A, Keiderling U, Macht M P and Wollenberger H 1996 *Mater. Sci. Forum* at press
[11] Busch R, Schneider S, Peker A and Johnson W L 1995 *Appl. Phys. Lett.* **67** 1544
[12] Schneider S, Thiyagarajan P and Johnson W L 1996 *Appl. Phys. Lett.* at press
[13] Keiderling U and Wiedenmann A 1995 *Physica* B **213** 895
[14] Glatter O and Kratky O 1982 *Small Angle X-ray Scattering* (London:Academic)
[15] Uebele P, Wiedenmann A, Herman H and Wetzig K 1996 *J. Appl. Crystallogr.* at press
[16] Fratzl P and Lebowitz J L 1989 *Acta Metall.* **37** 3245
[17] Langmayr F, Fratzl P and Vogl G 1992 *Acta Metall. Mater.* **40** 3381
[18] Budke E 1996 Private communication
[19] Sluchanko N E, Glushkov V V, Samarin N A and Brazhkin V V 1996 *Phys. Rev.* B at press
[20] Fratzl P and Blaschko O 1987 *Dynamics of Ordering Processes in Condensed Matter* ed S Komura and H Furukawa (New York: Plenum) p 223